

Hydrogen Atom in Relativistic Motion

M. Järvinen^{*,†}

Department of Physical Sciences and
Helsinki Institute of Physics
POB 64, FIN-00014 University of Helsinki, Finland

Abstract

The Lorentz contraction of bound states in field theory is often appealed to in qualitative descriptions of high energy particle collisions. Surprisingly, the contraction has not been demonstrated explicitly even in simple cases such as the hydrogen atom. It requires a calculation of wave functions evaluated at equal (ordinary) time for bound states in motion. Such wave functions are not obtained by kinematic boosts from the rest frame. Starting from the exact Bethe-Salpeter equation we derive the equal-time wave function of a fermion-antifermion bound state in QED, *i.e.*, positronium or the hydrogen atom, in any frame to leading order in α . We show explicitly that the bound state energy transforms as the fourth component of a vector and that the wave function of the fermion-antifermion Fock state contracts as expected. Transverse photon exchange contributes at leading order to the binding energy of the bound state in motion. We study the general features of the corresponding fermion-antifermion-photon Fock states, and show that they do not transform by simply contracting. We verify that the wave function reduces to the light-front one in the infinite momentum frame.

1 Introduction

Bound state wave functions are usually considered only in their center-of-mass frame, where rotational symmetry may be fully exploited. In the study of scattering amplitudes involving several bound states one needs, however, to know the wave functions in arbitrary Lorentz frames. Center-of-mass wave functions are commonly defined at equal time $t = 0$ of the constituents, and are non-trivially related to equal time wave functions in motion since the relative time is boost dependent [1]. Consequently, the Hamiltonian does not commute with the boost generators, causing the boost to be as complicated as solving the bound state equation directly in the new frame.

One manifestation of the non-trivial boost dynamics is the expectation, based on classical relativistic physics, that the equal-time wave function of a bound state in motion will be contracted in the direction of motion. High energy hadron scattering is thus often pictured as collisions between Lorentz-contracted pancakes. This is

^{*}Email address: Matti.O.Jarvinen@Helsinki.fi

[†]Research supported in part by the Academy of Finland through grant 102046.

necessarily a qualitative description since we are far from being able to calculate the wave function of a hadron even in the center-of-mass frame. However, it is surprising that the equal-time wave functions of much simpler bound states, such as the hydrogen atom, have apparently only been considered in the rest frame.

The hydrogen atom is a non-relativistic state (at leading order in the fine structure constant α) and the calculation of its wave function is one of the first exercises in courses on quantum mechanics. When the atom is in relativistic motion we must, however, make use of the full machinery of relativistic field theory. The excitation energies of Fock states with additional particles (electron-positron pairs, or photons) may be much less than the energy of the bound state. Hence the contributions of such higher Fock states must be carefully considered. As we shall see below, the exchange of transverse photons indeed contributes at leading order to the binding of hydrogen in motion. This is not unexpected, as a boost of the Coulomb potential leads to a transverse electromagnetic field.

The Lorentz contraction of 3+1 dimensional wave functions in gauge field theories has apparently not been demonstrated previously. In [1] a Lorentz contracting wave function of a two body QED bound state is represented as an approximation valid for small boosts. The frame dependence of bound state wave functions has been studied in various models, see for example, [2, 3, 4]. In [5, 6] Lorentz contraction is obtained for a fermion pair interacting via a δ potential. There has also been other interesting work on the Lorentz covariance of two body equations [7, 8].

It is reasonable to expect that the equal-time wave function of the hydrogen atom (or positronium) can be evaluated analytically in any frame to leading order in α . We find that the wave function of the e^+e^- Fock state indeed contracts as expected from classical relativity. The probability of the $e^+e^-\gamma$ state is of $\mathcal{O}(\alpha)$, which reflects the relative scarceness of photon exchange in the weak coupling limit. The photon amplitude does not classically contract, however. More generally, quantum fluctuations are unlikely to obey classical transformation laws.

Rather than trying to boost the well-known rest frame wave function of positronium we time order and solve its Bethe-Salpeter equation [9] for an arbitrary momentum of the bound state. We generalize our previous 1+1 dimensional calculation [10] by including the transverse photons which contribute in 3+1 dimensions. The equal-time formalism is of necessity Lorentz non-covariant – nevertheless we shall see that the bound state energy transforms as the fourth component of a Lorentz vector. We study the properties of the transverse photon distribution and show that it agrees with the light-front result in the limit of an infinitely large bound state momentum.

2 Wave equation for the hydrogen atom in motion

We calculate here the equal x^0 wave function for a (3+1 dimensional) fermion-antifermion bound state in the weak coupling limit $\alpha \ll 1$ of QED in any Lorentz frame. We will follow closely the procedure of [10] in 1+1 dimensions: the Bethe-Salpeter bound state equation is solved to leading order in α but to all orders in $|\mathbf{P}|/m$. Here \mathbf{P} is the total momentum of the system and the fermion masses m are taken to be equal for notational simplicity. We use Coulomb gauge ($\mathbf{k} \cdot \mathbf{A} = 0$), but also check that the result holds in Feynman gauge. In Coulomb gauge the unphysical

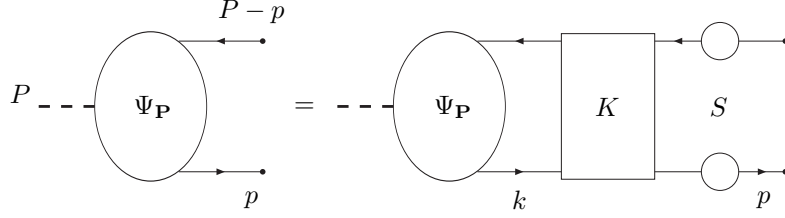


Figure 1: The Bethe-Salpeter equation. The blobs represent the wave function $\Psi_{\mathbf{P}}$, K is the interaction kernel and S is the two-particle propagator.

photon polarization states are absent and the contribution from physical, transverse polarizations is best seen.

Our starting point, the Bethe-Salpeter equation, is defined as shown in Fig. 1. The propagator S is the summed propagator including all radiative corrections. The interaction kernel K includes all two-particle irreducible interaction diagrams, *i.e.*, diagrams that cannot be split into two interaction graphs just by cutting two fermion lines. It is amputated such that it does not include the outgoing or incoming fermion propagators which are included in S . The Bethe-Salpeter wave function $\Psi_{\mathbf{P}}$ is defined as the projection of the bound state onto a fermion-antifermion state

$$\Psi_{\mathbf{P}}(p)_{\alpha\beta} = \int d^4x e^{ix \cdot p} \langle \Omega | T \{ \bar{\psi}_{\beta}(0) \psi_{\alpha}(x) \} | \mathbf{P} \lambda \rangle \quad (1)$$

where \mathbf{P} is the total momentum, p is the four momentum of the fermion, $\langle \Omega |$ is the vacuum of QED and λ represents all discrete quantum numbers of the bound state $| \mathbf{P} \lambda \rangle$ (such as spin and orbital angular momentum).

As in [10], we work in a time-ordered formalism where the Fock space structure of K and $\Psi_{\mathbf{P}}$ is seen explicitly. The time-ordered rules are obtained by taking a Fourier transform over p^0 . The fermion propagator has forward and backward moving parts in (t, \mathbf{p}) space

$$\begin{aligned} S_F(t, \mathbf{p}) &\equiv \int \frac{dp^0}{2\pi} \exp(-itp^0) \frac{i}{\not{p} - m + i\epsilon} \\ &= \Theta(t) \Lambda^+(\mathbf{p}) \exp(-itE_{\mathbf{p}}) + \Theta(-t) \Lambda^-(-\mathbf{p}) \exp(itE_{\mathbf{p}}) \end{aligned} \quad (2)$$

where $E_{\mathbf{p}} = \sqrt{\mathbf{p}^2 + m^2}$ and the projection operators Λ^{\pm} are defined by

$$\Lambda^{\pm}(\mathbf{p}) \equiv \frac{\pm \gamma^0 E_{\mathbf{p}} \mp \boldsymbol{\gamma} \cdot \mathbf{p} + m}{2E_{\mathbf{p}}} . \quad (3)$$

Similarly, the photon propagator in (t, \mathbf{p}) space reads in Feynman gauge

$$D_F^{\mu\nu}(t, \mathbf{p}) = -\frac{g^{\mu\nu}}{2|\mathbf{p}|} [\Theta(t) \exp(-i|\mathbf{p}|t) + \Theta(-t) \exp(i|\mathbf{p}|t)] . \quad (4)$$

In Coulomb gauge ($\mathbf{p} \cdot \mathbf{A} = 0$) we have an instantaneous contribution from the D^{00} component

$$\begin{aligned} D_C^{00}(t, \mathbf{p}) &= \delta(t) \frac{i}{\mathbf{p}^2} ; \quad D_C^{i0} = D_C^{0i} = 0 \\ D_C^{ij}(t, \mathbf{p}) &= \left(\delta^{ij} - \frac{p^i p^j}{\mathbf{p}^2} \right) \frac{1}{2|\mathbf{p}|} [\Theta(t) \exp(-i|\mathbf{p}|t) + \Theta(-t) \exp(i|\mathbf{p}|t)] . \end{aligned} \quad (5)$$

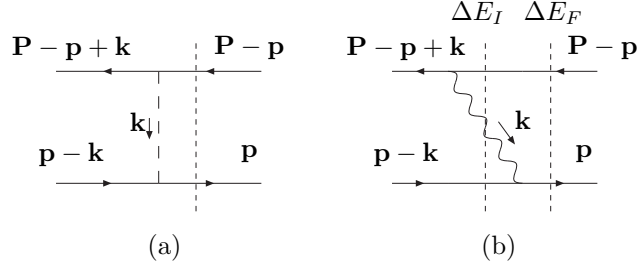


Figure 2: Time-ordered single photon exchange diagrams which arise from the interaction kernel K of Fig. 1. (a) The instantaneous Coulomb interaction K_γ^a . (b) The exchange of a transverse photon K_γ^b . Time flows to the right.

In the usual time-ordered perturbation theory one integrates over all time differences from zero to infinity. The integrals give energy denominators which are denoted by vertical cuts in the Feynman diagrams in the following sections.

In the center-of-mass frame of positronium the scale of the internal momenta and the scale of the binding energy or the potential energy are

$$|\mathbf{p}| \sim \alpha m, \quad \Delta E \sim V \sim \alpha^2 m, \quad (6)$$

respectively. For a moving system we define the relative momentum by

$$\mathbf{q} \equiv \mathbf{p} - \mathbf{P}/2. \quad (7)$$

We expect the transverse components of \mathbf{q} and of the photon momentum \mathbf{k} to be the same order as in the rest frame (6), whereas the longitudinal components and the energy differences will be affected by the contraction,

$$q_{\parallel} \sim k_{\parallel} \sim \gamma \alpha m, \quad |\mathbf{q}_{\perp}| \sim |\mathbf{k}_{\perp}| \sim \alpha m, \quad \Delta E \sim \gamma^{-1} \alpha^2 m \quad (8)$$

where $\gamma \equiv \sqrt{\mathbf{P}^2 + (2m)^2}/2m$ is the boost parameter of the bound state (to lowest order in α).

2.1 Structure of the interaction kernel

Next we will identify the leading contributions to K using time-ordered diagrams in the weak coupling limit. We will see that they arise from the single photon exchange part of K which involves only Fock states with one additional photon. The radiative corrections to the fermion propagators which are included in S of Fig. 1 renormalize the mass and change the off-shell dependence of the propagator. In a non-relativistic bound state the constituents are nearly on-shell. Hence to leading order in α these effects are accounted for by using the physical mass m in the propagator (2).

When iterated the Bethe-Salpeter equation (Fig. 1) gives the wave function as an infinite ladder diagram with rungs composed of the kernel K . We will time order the ladder and analyze its blocks. We work here in Coulomb gauge, but it is easy to check that the results are gauge independent.

Let us first analyze the single photon exchange diagrams (Fig. 2). Using time-ordered Feynman rules in Coulomb gauge, we have

$$\begin{aligned}
K_\gamma^a &= \frac{i}{E - E_{\mathbf{p}} - E_{\mathbf{p}-\mathbf{p}}} \int \frac{d^3\mathbf{k}}{(2\pi)^3} \frac{i}{\mathbf{k}^2} \\
&\quad \cdot \Lambda^+(\mathbf{p}) i e \gamma^0 \Lambda^+(\mathbf{p}-\mathbf{k}) \otimes \Lambda^-(\mathbf{P}-\mathbf{p}+\mathbf{k}) i e \gamma^0 \Lambda^-(\mathbf{P}-\mathbf{p}) \\
K_\gamma^b &= \frac{i}{E - E_{\mathbf{p}} - E_{\mathbf{p}-\mathbf{p}}} \int \frac{d^3\mathbf{k}}{(2\pi)^3} \frac{1}{2|\mathbf{k}|} \frac{i}{E - E_{\mathbf{p}-\mathbf{k}} - E_{\mathbf{p}-\mathbf{p}} - |\mathbf{k}|} \\
&\quad \cdot \left(\delta^{ij} - \frac{k^i k^j}{\mathbf{k}^2} \right) \Lambda^+(\mathbf{p}) i e \gamma^i \Lambda^+(\mathbf{p}-\mathbf{k}) \otimes \Lambda^-(\mathbf{P}-\mathbf{p}+\mathbf{k}) i e \gamma^j \Lambda^-(\mathbf{P}-\mathbf{p})
\end{aligned} \tag{9}$$

where \otimes denotes a direct product between the Dirac spaces of the fermions. For the energy denominators arising from the cuts of Fig. 2 we have [using (7) and (8)]¹

$$\Delta E_F \equiv E - E_{\mathbf{p}} - E_{\mathbf{p}-\mathbf{p}} \sim \Delta E \sim \alpha^2 m \gamma^{-1} \tag{10}$$

$$\begin{aligned}
\Delta E_I &\equiv E - E_{\mathbf{p}-\mathbf{k}} - E_{\mathbf{p}-\mathbf{p}} - |\mathbf{k}| = E - E_{\mathbf{p}} - E_{\mathbf{p}-\mathbf{p}} + (E_{\mathbf{p}} - E_{\mathbf{p}-\mathbf{k}} - |\mathbf{k}|) \\
&\sim (E_{\mathbf{p}} - E_{\mathbf{p}-\mathbf{k}} - |\mathbf{k}|) \sim \alpha m \gamma^{-1} .
\end{aligned} \tag{11}$$

From (10) we have for the energy differences $\Delta E_F \simeq \alpha \Delta E_I$: for the excitation of one photon we need an energy $\mathcal{O}(1/\alpha)$ higher than the binding energy in all frames. Correspondingly, for the time scales $\Delta t_{I/F} \equiv 1/\Delta E_{I/F}$ we have $\Delta t_I \simeq \alpha \Delta t_F$. Hence transverse photon exchange is a rare event in the weak coupling limit: The probability of finding the bound state in an excited Fock state should be the ratio of the two time scales and thus $\sim \alpha$. This expectation will be confirmed in Sec. 3.

In Fig. 2 and in the above analysis we assumed that all the fermions move forward in time. However, the fermion propagator (2) also contains a backward moving component. Its inclusion leads to “Z graphs” involving pair production which are suppressed in the non-relativistic limit due to large energy denominators.

Let us pay attention to the coupling structure appearing in (9). Recalling the definition of Λ^\pm in (3), we use the property $\{\gamma^\mu, \gamma^\nu\} = 2g^{\mu\nu}$ to write

$$\Lambda^+(\mathbf{p}-\mathbf{k}) \gamma^\mu \Lambda^+(\mathbf{p}) = \Lambda^+(\mathbf{p}-\mathbf{k}) \left[\frac{p^\mu}{E_{\mathbf{p}}} + \Lambda^-(\mathbf{p}) \gamma^\mu \right] . \tag{12}$$

Using $\Lambda^+(\mathbf{p}) \Lambda^-(\mathbf{p}) = 0$ and the results (7), (8) we can estimate

$$\begin{aligned}
\Lambda^+(\mathbf{p}-\mathbf{k}) \Lambda^-(\mathbf{p}) &= \mathcal{O}(|\mathbf{k}|/\mathcal{E}) = \mathcal{O}(\alpha) \\
\frac{p^\mu}{E_{\mathbf{p}}} &= \frac{P^\mu}{\mathcal{E}} + \mathcal{O}(\alpha)
\end{aligned} \tag{13}$$

where $P^0 \simeq \mathcal{E} \equiv \sqrt{(2m)^2 + \mathbf{P}^2}$. Inserting (13) into (12) we have

$$\Lambda^+(\mathbf{p}-\mathbf{k}) \gamma^\mu \Lambda^+(\mathbf{p}) = \Lambda^+(\mathbf{p}-\mathbf{k}) \frac{P^\mu}{\mathcal{E}} + \mathcal{O}(\alpha) . \tag{14}$$

¹We will see that the scaling behavior γ^{-1} of ΔE_F is an exact result whereas $\Delta E_I \propto \gamma^{-1}$ holds for $k_{\parallel} > 0$. For $k_{\parallel} < 0$ we would have $\Delta E_I \sim \gamma \alpha m$. This reflects the fact that for $\gamma \gg 1$ backward moving photons are suppressed, see Sec. 3.

A similar analysis for the antifermion coupling reveals that at leading order we may replace

$$\begin{aligned}\gamma^\mu \Lambda^+(\mathbf{p}) &\longrightarrow \frac{P^\mu}{\mathcal{E}} \\ \Lambda^-(\mathbf{P}-\mathbf{p})\gamma^\mu &\longrightarrow -\frac{P^\mu}{\mathcal{E}}.\end{aligned}\quad (15)$$

Using the above estimates we can see that in a general frame both diagrams of Fig. 2 are of the same order in α . Let us first analyze diagram (a). The first factor in Eq. (9) gives $\Delta t_F \sim \gamma \alpha^{-2} m^{-1}$. Using (15) we have

$$\Lambda^+(\mathbf{p})\gamma^0 \otimes \gamma^0 \Lambda^-(\mathbf{P}-\mathbf{p}) \sim \left(\frac{P^0}{\mathcal{E}}\right)^2 \simeq 1. \quad (16)$$

The Coulomb potential gives using (8)

$$\alpha \int \frac{d^3\mathbf{k}}{(2\pi)^3} \frac{1}{\mathbf{k}^2} \sim \alpha \frac{\mathbf{k}_\perp^2 k_\parallel}{|\mathbf{k}|^2} \sim \gamma^{-1} \alpha^2 m \equiv V. \quad (17)$$

Altogether

$$K_\gamma^a \sim \Delta t_F \cdot V \sim \gamma \alpha^{-2} m^{-1} \cdot \gamma^{-1} \alpha^2 m = \alpha^0 \quad (18)$$

where we dropped the k dependent projectors $\Lambda^+(\mathbf{p}-\mathbf{k})$ and $\Lambda^-(\mathbf{P}-\mathbf{p}+\mathbf{k})$ which belong to a different block of $K \cdot S$ (see Fig. 1). For diagram (b)

$$\left(\delta^{ij} - \frac{k^i k^j}{\mathbf{k}^2}\right) \Lambda^+(\mathbf{p})\gamma^i \otimes \gamma^j \Lambda^-(\mathbf{P}-\mathbf{p}) \sim \left(\delta^{ij} - \frac{k^i k^j}{\mathbf{k}^2}\right) \frac{P^i P^j}{\mathcal{E} \mathcal{E}} = \beta^2 \frac{\mathbf{k}_\perp^2}{\mathbf{k}^2} \sim \frac{\beta^2}{\gamma^2} \quad (19)$$

where $\beta \equiv |\mathbf{P}|/\mathcal{E}$. The potential contributes

$$\alpha \int \frac{d^3\mathbf{k}}{(2\pi)^3} \frac{1}{2|\mathbf{k}|} \frac{i}{E - E_{\mathbf{p}} - E_{\mathbf{P}-\mathbf{p}+\mathbf{k}} - |\mathbf{k}|} \sim \alpha \Delta t_I \frac{\mathbf{k}_\perp^2 k_\parallel}{|\mathbf{k}|} \sim \gamma \alpha^2 m \quad (20)$$

and thus

$$K_\gamma^b \sim \gamma \alpha^{-2} m^{-1} \cdot \beta^2 \gamma^{-2} \cdot \gamma \alpha^2 m = \beta^2 \alpha^0. \quad (21)$$

In particular, due to the couplings (19), the contribution from transverse photons [Fig. 2 (b)] is absent at order α^0 in the center-of-mass frame ($\beta = 0$). This is the expected result: for the hydrogen atom at rest transverse photons do not contribute at leading order, but appear as spin dependent interactions at next-to-leading order. The spin dependent interactions are hidden in the $\mathcal{O}(\alpha)$ terms of (14) also when $\mathbf{P} \neq 0$.

Next we will show that more complicated diagrams can be neglected in all frames. A representative set of two photon exchange diagrams is shown in Fig. 3. Diagram (a) will be included in our approximation. Diagrams (b) and (d) which include Fock states with two photons and diagram (c) will be suppressed.

Let us study more closely diagrams (a) and (b). Diagram (a) simply consists of two separate transverse photon exchanges of Fig. 2(a), and we have from (18)

$$K_{\gamma\gamma}^a \sim (K_\gamma^b)^2 \sim \beta^4 \alpha^0. \quad (22)$$

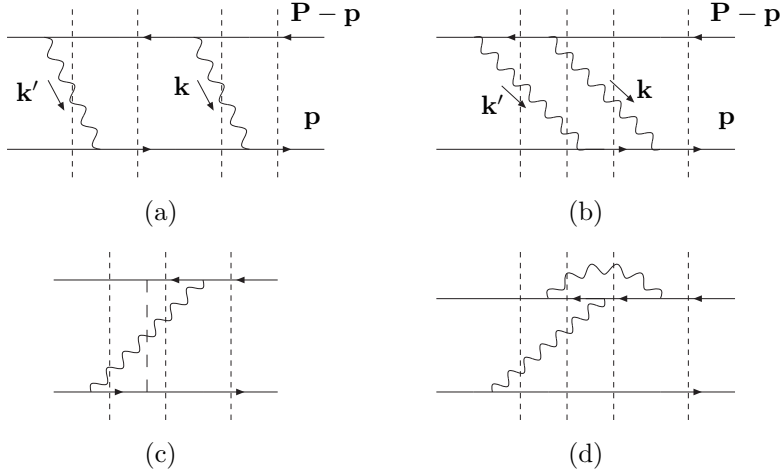


Figure 3: Time-ordered two photon exchange diagrams. Diagrams (a) and (b) arise from iterating the covariant Bethe-Salpeter equation (Fig. 1) with one photon exchange kernels. Diagrams (c) and (d) arise from two photon kernels.

However, in diagram (b) three of the cuts intersect photon lines instead of two. Quantitatively, the only difference to diagram (a) comes from the second cut from the left:

$$\begin{aligned}
 (a) : \quad & \frac{1}{E - E_{\mathbf{p}-\mathbf{k}} - E_{\mathbf{P}-\mathbf{p}+\mathbf{k}}} \sim \gamma \alpha^{-2} m^{-1} = \Delta t_F \\
 (b) : \quad & \frac{1}{E - E_{\mathbf{p}} - E_{\mathbf{P}-\mathbf{p}+\mathbf{k}+\mathbf{k}'} - |\mathbf{k}| - |\mathbf{k}'|} \lesssim \gamma \alpha^{-1} m^{-1} = \Delta t_I . \quad (23)
 \end{aligned}$$

That is, in diagram (a) the two interactions are separated by the long time scale Δt_F , but in diagram (b) both the interactions must occur within the shorter time scale Δt_I . We have

$$K_{\gamma\gamma}^b \sim \frac{\Delta t_I}{\Delta t_F} K_{\gamma\gamma}^a \sim \beta^4 \alpha \quad (24)$$

and the diagram is thus suppressed. The qualitative picture is that the flight time of a photon is short compared to the intervals between the exchanges. Thus the probability of having two photons at the same instant of time is low. Similar arguments show that diagrams (c) and (d) are also suppressed.

In the case of positronium the kernel K includes annihilation diagrams with, *e.g.*, one photon as an intermediate Fock state. Similar arguments as above show that these graphs are $\mathcal{O}(\alpha^2)$ and thus suppressed in all frames.

We assumed in this section that momenta of order $|\mathbf{k}_\perp| \sim \alpha m$ (and $k_\parallel \sim \gamma \alpha m$) dominate the integrations, which is true at leading order in α . Transverse photons with softer momenta $|\mathbf{k}_\perp| \sim \alpha^2 m$ are suppressed by $\mathcal{O}(\alpha)$ due to the smaller phase space. However, the flight time of such photons is comparable with the longer time scale Δt_F . This allows an arbitrary number of harder $|\mathbf{k}_\perp| \sim \alpha m$ (transverse or Coulomb) exchanges while the soft photon is in flight. As the harder interactions are $\mathcal{O}(\alpha^0)$ contributions, the diagrams similar to the one shown in Fig. 3(c) but with, *e.g.*, several Coulomb exchanges are in fact all $\mathcal{O}(\alpha)$. Such diagrams are known to contribute to bound state structure at higher orders in the center-of-mass frame [11].

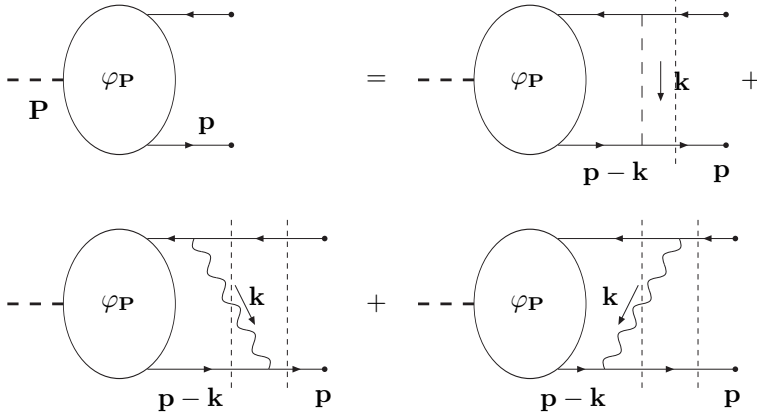


Figure 4: The time-ordered bound state equation in the ladder approximation. The blobs denote the equal-time wave function $\varphi_{\mathbf{P}}$ defined in (25).

2.2 Lorentz contraction of the e^+e^- wave function

Now we are ready to write the bound state equation (Fig. 1) in time-ordered form with only the leading diagrams included. After the Fourier transform over energy, the relevant wave function is the equal-time wave function

$$\varphi_{\mathbf{P}}(\mathbf{p})_{\alpha\beta} \equiv \int \frac{dp^0}{2\pi} \Psi_{\mathbf{P}}(p)_{\alpha\beta}. \quad (25)$$

The equation is shown in Fig. 4. The analytic expression reads

$$\begin{aligned} \varphi_{\mathbf{P}}(\mathbf{p}) &= \frac{i}{E - E_{\mathbf{p}} - E_{\mathbf{P}-\mathbf{p}}} \int \frac{d^3\mathbf{k}}{(2\pi)^3} \left[\frac{i}{\mathbf{k}^2} \Lambda^+(\mathbf{p}) i e \gamma^0 \varphi_{\mathbf{P}}(\mathbf{p}-\mathbf{k}) i e \gamma^0 \Lambda^-(\mathbf{P}-\mathbf{p}) \right. \\ &+ \left(\frac{i}{E - E_{\mathbf{p}-\mathbf{k}} - E_{\mathbf{P}-\mathbf{p}} - |\mathbf{k}|} + \frac{i}{E - E_{\mathbf{p}} - E_{\mathbf{P}-\mathbf{p}+\mathbf{k}} - |\mathbf{k}|} \right) \\ &\cdot \left. \frac{1}{2|\mathbf{k}|} \left(\delta^{ij} - \frac{k^i k^j}{\mathbf{k}^2} \right) \Lambda^+(\mathbf{p}) i e \gamma^i \varphi_{\mathbf{P}}(\mathbf{p}-\mathbf{k}) i e \gamma^j \Lambda^-(\mathbf{P}-\mathbf{p}) \right] \end{aligned} \quad (26)$$

where $\varphi_{\mathbf{P}}$ is understood as a 4x4 Dirac matrix. In particular, from the property $\Lambda^\pm \Lambda^\mp = 0$ of the projection matrices (3) it follows that

$$\Lambda^-(\mathbf{p}) \varphi_{\mathbf{P}}(\mathbf{p}) = 0 = \varphi_{\mathbf{P}}(\mathbf{p}) \Lambda^+(\mathbf{P}-\mathbf{p}), \quad (27)$$

i.e., the wave function (25) has only forward moving components in the weak coupling limit.

At leading order in α we may use the replacement (15) to eliminate the Dirac structure. We have

$$\begin{aligned} \varphi_{\mathbf{P}}(\mathbf{p}) &= \frac{-e^2}{E - E_{\mathbf{p}} - E_{\mathbf{P}-\mathbf{p}}} \int \frac{d^3\mathbf{k}}{(2\pi)^3} \left[\frac{1}{\mathbf{k}^2} + \frac{1}{\mathcal{E}^2} \left(\mathbf{P}^2 - \frac{(\mathbf{P} \cdot \mathbf{k})^2}{\mathbf{k}^2} \right) \frac{1}{2|\mathbf{k}|} \right. \\ &\cdot \left. \left(\frac{1}{E - E_{\mathbf{p}} - E_{\mathbf{P}-\mathbf{p}+\mathbf{k}} - |\mathbf{k}|} + \frac{1}{E - E_{\mathbf{p}-\mathbf{k}} - E_{\mathbf{P}-\mathbf{p}} - |\mathbf{k}|} \right) \right] \varphi_{\mathbf{P}}(\mathbf{p}-\mathbf{k}) \end{aligned} \quad (28)$$

$$\equiv \frac{1}{E - E_{\mathbf{p}} - E_{\mathbf{p}-\mathbf{k}}} \int \frac{d^3\mathbf{k}}{(2\pi)^3} V(\mathbf{k}) \varphi_{\mathbf{p}}(\mathbf{p} - \mathbf{k}) \quad (29)$$

where $\mathcal{E} \equiv \sqrt{\mathbf{P}^2 + (2m)^2}$. The equation thus reduces to a scalar equation for the forward moving components of $\varphi_{\mathbf{p}}$. In comparison with the 1+1 dimensional equation of Ref. [10], we now have a contribution from transverse photon exchange.

Let us study the sum $E_{\mathbf{p}} + E_{\mathbf{p}-\mathbf{k}}$ appearing in the denominator of (29). Expanding in the relative momentum \mathbf{q} of (7) we get

$$E_{\mathbf{p}} + E_{\mathbf{p}-\mathbf{k}} - \mathcal{E} = \frac{1}{2\mu\gamma} \left(\mathbf{q}_{\perp}^2 + \gamma^{-2} q_{\parallel}^2 \right) + \mathcal{O}(\gamma^{-1} \alpha^4 m) \quad (30)$$

where $\gamma \equiv \mathcal{E}/2m$ and $\mu \equiv m/2$. Note that the form of (30) is consistent with our expectation (8). For the energy denominators in the transverse part of (28) we get

$$\begin{aligned} E - E_{\mathbf{p}-\mathbf{k}} - E_{\mathbf{p}-\mathbf{k}} - |\mathbf{k}| &= (E - E_{\mathbf{p}} - E_{\mathbf{p}-\mathbf{k}}) + (E_{\mathbf{p}} - E_{\mathbf{p}-\mathbf{k}} - |\mathbf{k}|) \\ &= \frac{\mathbf{P} \cdot \mathbf{k}}{\mathcal{E}} - |\mathbf{k}| + \mathcal{O}(\gamma^{-1} \alpha^2 m) \\ E - E_{\mathbf{p}} - E_{\mathbf{p}-\mathbf{k}+\mathbf{k}} - |\mathbf{k}| &= -\frac{\mathbf{P} \cdot \mathbf{k}}{\mathcal{E}} - |\mathbf{k}| + \mathcal{O}(\gamma^{-1} \alpha^2 m) \end{aligned} \quad (31)$$

and the potential defined in (29) becomes

$$\frac{1}{4\pi\alpha} V(\mathbf{k}) = -\frac{1}{\mathbf{k}^2} + \frac{\beta^2 \mathbf{k}_{\perp}^2}{2\mathbf{k}^2} \left(\frac{1}{\mathbf{k}^2 + \beta k_{\parallel} |\mathbf{k}|} + \frac{1}{\mathbf{k}^2 - \beta k_{\parallel} |\mathbf{k}|} \right) \quad (32)$$

$$= -\frac{1}{\mathbf{k}^2} + \frac{\beta^2 \mathbf{k}_{\perp}^2}{\mathbf{k}^2 (\mathbf{k}_{\perp}^2 + \gamma^{-2} k_{\parallel}^2)} = -\frac{1}{\gamma^2 (\mathbf{k}_{\perp}^2 + \gamma^{-2} k_{\parallel}^2)} \quad (33)$$

in terms of the parallel and perpendicular components of \mathbf{k} and with $\beta \equiv |\mathbf{P}|/\mathcal{E}$. In particular, the contribution from the transverse photons [second term in (32)] is proportional to β^2 and vanishes in the center-of-mass frame. Requiring the potential energy (33) to be commensurate with the relative kinetic energy in (30) finally verifies our expectation (8) and the γ dependence of the non-leading terms in (30), (31).

Let us define the binding energy $\Delta M \equiv \sqrt{E^2 - \mathbf{P}^2} - 2m$ which should be independent of \mathbf{P} . As $E - \mathcal{E} = \Delta E \sim \gamma^{-1} \alpha^2 m$, we have

$$\Delta M = \gamma(E - \mathcal{E}) + \mathcal{O}(\alpha^4 m) . \quad (34)$$

Inserting (30), (33) and (34) into (29) we get

$$\left[\Delta M - \frac{1}{2\mu} \left(\mathbf{q}_{\perp}^2 + \gamma^{-2} q_{\parallel}^2 \right) \right] \varphi_{\mathbf{p}}(\mathbf{p}) = -\frac{4\pi\alpha}{\gamma} \int \frac{d^3\mathbf{k}}{(2\pi)^3} \frac{\varphi_{\mathbf{p}}(\mathbf{p} - \mathbf{k})}{\mathbf{k}_{\perp}^2 + \gamma^{-2} k_{\parallel}^2} . \quad (35)$$

We see that all frame dependence, *i.e.*, the γ factors, can be removed by rescaling $k_{\parallel} \rightarrow \gamma k_{\parallel}$ and $q_{\parallel} \rightarrow \gamma q_{\parallel}$. Then the spectrum is given by the same Schrödinger equation as in the center-of-mass frame. The e^+e^- wave function exactly Lorentz contracts (or expands in \mathbf{k} space) in the direction of motion. Taking into account the Dirac structure (27), the result can be written

$$\varphi_{\mathbf{p}}(\mathbf{p})_{\alpha\beta} = \sum_{s_1, s_2} \frac{u_{\alpha}(\mathbf{P}/2, s_1) \bar{v}_{\beta}(\mathbf{P}/2, s_2)}{2E_{\mathbf{P}/2}} \chi_{s_1, s_2} \phi_{\mathbf{p}}(\mathbf{q}) \quad (36)$$

where u, v are the usual Dirac spinors and $\phi_{\mathbf{P}}$ is given by Lorentz contracting the usual wave function ϕ_{CM} of the hydrogen atom at rest:

$$\phi_{\mathbf{P}}(\mathbf{q}) = \frac{1}{\sqrt{\gamma}} \phi_{CM}(\mathbf{q}_{\perp}, q_{\parallel}/\gamma). \quad (37)$$

The spin wave function χ is normalized as $\sum_{s_1, s_2} |\chi_{s_1, s_2}|^2 = 1$. At leading order in α we were able to replace \mathbf{p} and $\mathbf{P} - \mathbf{p}$ by $\mathbf{P}/2$ in the Dirac structure of (36).

We finally check that the result (36) is also obtained in Feynman gauge with the propagator (4). In this gauge the photon propagator has no instantaneous part and (26) becomes

$$\begin{aligned} \varphi_{\mathbf{P}}(\mathbf{p}) &= \frac{i}{E - E_{\mathbf{p}} - E_{\mathbf{P}-\mathbf{p}}} \int \frac{d^3\mathbf{k}}{(2\pi)^3} \Lambda^+(\mathbf{p}) i e \gamma^{\mu} \varphi_{\mathbf{P}}(\mathbf{p} - \mathbf{k}) i e \gamma_{\mu} \Lambda^-(\mathbf{P} - \mathbf{p}) \\ &\cdot \frac{-1}{2|\mathbf{k}|} \left(\frac{i}{E - E_{\mathbf{p}-\mathbf{k}} - E_{\mathbf{P}-\mathbf{p}} - |\mathbf{k}|} + \frac{i}{E - E_{\mathbf{p}} - E_{\mathbf{P}-\mathbf{p}+\mathbf{k}} - |\mathbf{k}|} \right). \end{aligned} \quad (38)$$

Using (15), the Dirac structure reduces to a factor $-\gamma^{-2}$. Further using (31), the potential in Feynman gauge becomes

$$\frac{1}{4\pi\alpha} V(\mathbf{k}) = -\frac{1}{\gamma^2} \cdot \frac{1}{2} \left(\frac{1}{\mathbf{k}^2 + \beta k_{\parallel} |\mathbf{k}|} + \frac{1}{\mathbf{k}^2 - \beta k_{\parallel} |\mathbf{k}|} \right) = -\frac{1}{\gamma^2 (\mathbf{k}_{\perp}^2 + \gamma^{-2} k_{\parallel}^2)} \quad (39)$$

which is the same result as in Coulomb gauge (33). The rest of the calculation remains unchanged.

3 The $e^+e^- \gamma$ wave function

In the preceding section we derived the wave function for the e^+e^- Fock state, which is expected to be the leading component of the bound state in the weak coupling limit. Now we will analyze the wave function of the $e^+e^- \gamma$ Fock state: we calculate the distribution of physical, transverse photons in the bound state. We will see that this state occurs with a probability $\mathcal{O}(\alpha)$, whereas Fock states with more photons or e^+e^- pairs contribute terms of $\mathcal{O}(\alpha^2)$ to the normalization.

The $e^+e^- \gamma$ Fock state contributes as an intermediate state in the derivation of (35), see Fig. 4. However, to clarify the derivation of its wavefunction it is best to start again from the exact covariant formalism: we will briefly repeat the analysis of the previous section but now for the $e^+e^- \gamma$ Fock state. The photon distribution will be related to the square of the equal-time wave function of the Fock state just as in usual non-relativistic quantum mechanics. For an analogous calculation on the light-front see [12, 13].

Let us define the wave function as a coupling to an $e^+e^- \gamma$ state

$$\Psi_{\gamma \mathbf{P}}(p, k) \equiv \int d^4x d^4y e^{+ix \cdot (p-k) + iy \cdot k} \langle \Omega | T \{ \bar{\psi}_{\beta}(0) \psi_{\alpha}(x) A^{\mu}(y) \} | \mathbf{P} \lambda \rangle. \quad (40)$$

A covariant equation analogous to the Bethe-Salpeter equation connecting Ψ_{γ} to the wave function Ψ of (1) may be derived in a way analogous to the derivation of the

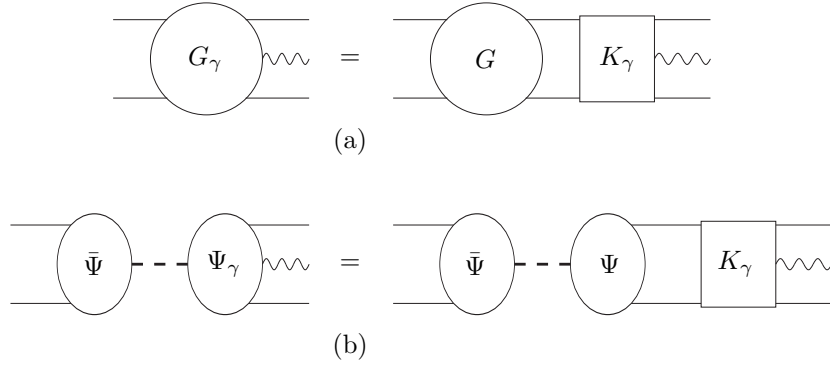


Figure 5: Derivation of the Bethe-Salpeter equation for the photon wave function. (a) The generating equation for the five-point Green function. G is the four-fermion Green function, G_γ has in addition a photon insertion and K_γ is the two-particle irreducible kernel. (b) The pole contribution giving the Bethe-Salpeter equation. Arrows on the quark lines were dropped for simplicity.

original Bethe-Salpeter equation (see [9, 14]). We only sketch the proof here (see Fig. 5). The five-point Green function G_γ satisfies the identity shown in Fig. 5a which may be proved diagrammatically. The kernel K_γ is defined to be the sum of all two-particle irreducible diagrams, *i.e.*, diagrams which cannot be divided into two separate diagrams by cutting two fermion lines. The wave equation is then obtained by calculating the residues at the pole caused by the bound state (see Fig. 5b), *i.e.*, at $P^2 = M^2$, where P is the total momentum and M is the bound state mass. Ψ_γ is simply given by adding the kernel K_γ to Ψ . Note that K_γ cannot have a pole at $P^2 = M^2$: this would lead to G_γ having a double pole.

Let us move to the time-ordered formalism. The equal-time wave function for the single photon Fock state may be defined as

$$\begin{aligned}
\Phi_{\mathbf{P}}^\mu(\mathbf{p}, \mathbf{k}) &\equiv \int \frac{dp^0}{2\pi} \frac{dk^0}{2\pi} \Psi_{\gamma \mathbf{P}}(p, k) \\
&= \int d^3\mathbf{x} d^3\mathbf{y} e^{-i\mathbf{x}\cdot(\mathbf{p}-\mathbf{k}) - i\mathbf{y}\cdot\mathbf{k}} \langle \Omega | \bar{\psi}_\beta(0) \psi_\alpha(x) A^\mu(y) | \mathbf{P} \lambda \rangle \Big|_{x^0=y^0=0} \\
&\equiv \langle \Omega | \bar{\psi}_\beta(0) \tilde{\psi}_\alpha(\mathbf{p}-\mathbf{k}) \tilde{A}^\mu(\mathbf{k}) | \mathbf{P} \lambda \rangle .
\end{aligned} \tag{41}$$

When time ordered, the interaction K_γ gives rise to several graphs of which some are shown in Fig. 6. Diagram (c) arises in fact as a combination of the lowest order kernels K and K_γ , but will be suppressed since the two photons overlap in time.

Similarly as in Sec. 2.1 we find that diagram (a) together with a similar diagram in which the photon is emitted by the antifermion gives the leading contribution in α . Thus at leading order in α the wave function (41) is related to $\varphi_{\mathbf{P}}$ of (25) as shown in Fig. 7. The analytic expression is in Coulomb gauge

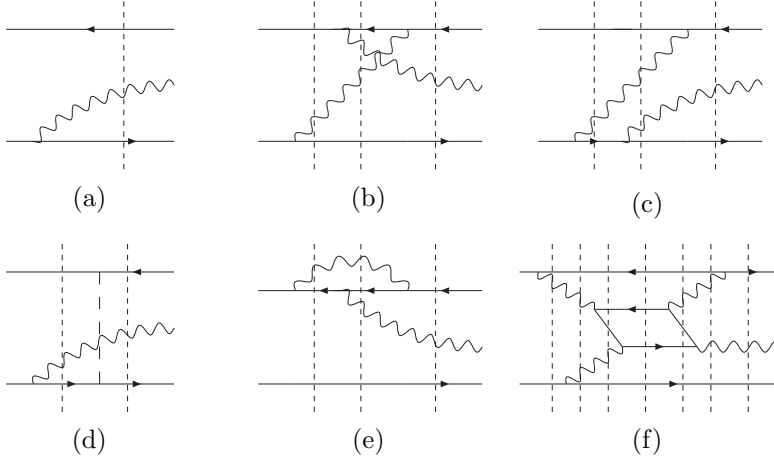


Figure 6: Time-ordered diagrams arising from the interaction kernel K_γ . (a) is a leading diagram in α .

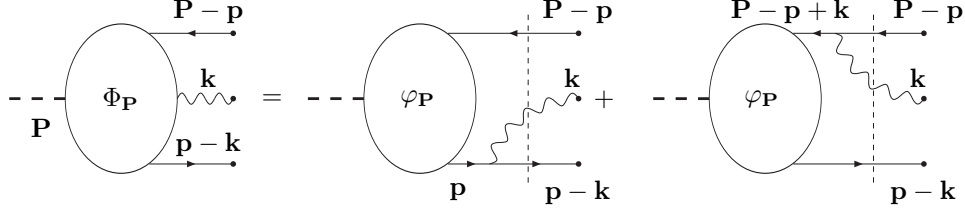


Figure 7: The calculation of the $e^+e^-\gamma$ wave function.

$$\Phi_{\mathbf{P}}^i(\mathbf{p}, \mathbf{k}) = \frac{i}{E - E_{\mathbf{p}-\mathbf{k}} - E_{\mathbf{P}-\mathbf{p}} - |\mathbf{k}|} \frac{1}{2|\mathbf{k}|} \left(\delta^{ij} - \frac{k^i k^j}{\mathbf{k}^2} \right) \cdot [\varphi_{\mathbf{P}}(\mathbf{p}) ie\gamma^j \Lambda^+(\mathbf{p}-\mathbf{k}) + \Lambda^-(\mathbf{P}-\mathbf{p}) ie\gamma^j \varphi_{\mathbf{P}}(\mathbf{p}-\mathbf{k})] . \quad (42)$$

To find the behavior of $\Phi_{\mathbf{P}}^i$ for the scales of \mathbf{k} and \mathbf{q} which are relevant in the bound state, we may use the previous analysis to simplify the expression. Using (10) and (15) we have

$$\Phi_{\mathbf{P}}^i(\mathbf{p}, \mathbf{k}) = \frac{e}{2\mathbf{k}^2 - 2\beta k_{\parallel} |\mathbf{k}|} \left(\frac{P^i}{\mathcal{E}} - \frac{k^i \beta k_{\parallel}}{\mathbf{k}^2} \right) (\varphi_{\mathbf{P}}(\mathbf{p}) - \varphi_{\mathbf{P}}(\mathbf{p}-\mathbf{k})) [1 + \mathcal{O}(\alpha)] . \quad (43)$$

To give a probabilistic interpretation for the result (43) we need to define the normalization of the wave functions. We take the normalization of the bound state to be the “non-relativistic” one (without a $2\mathcal{E}$ factor) so that

$$\langle \mathbf{P}' \lambda' | \mathbf{P} \lambda \rangle = (2\pi)^3 \delta^{(3)}(\mathbf{P}' - \mathbf{P}) \delta_{\lambda' \lambda} . \quad (44)$$

Then we have

$$1 = \sum_{\lambda'} \int \frac{d^3 \mathbf{P}'}{(2\pi)^3} \langle \mathbf{P}' \lambda' | \mathbf{P} \lambda \rangle = \sum_{\lambda'} \int \frac{d^3 \mathbf{P}'}{(2\pi)^3} \langle \mathbf{P}' \lambda' | \mathbf{1}_{f\bar{f}} + \mathbf{1}_{f\bar{f}\gamma} + \dots | \mathbf{P} \lambda \rangle \quad (45)$$

where the $\mathbf{1}$'s are projection operators on different Fock states², *e.g.*,

$$\begin{aligned}
\mathbf{1}_{f\bar{f}\gamma} &= \int \frac{d^3\mathbf{p}_1}{(2\pi)^3} \frac{d^3\mathbf{p}_2}{(2\pi)^3} \frac{d^3\mathbf{k}}{(2\pi)^3} \sum_{s_1, s_2, \lambda} c_{s_1}^\dagger(\mathbf{p}_1) d_{s_2}^\dagger(\mathbf{p}_2) a_\lambda^\dagger(\mathbf{k}) |0\rangle \langle 0| c_{s_1}(\mathbf{p}_1) d_{s_2}(\mathbf{p}_2) a_\lambda(\mathbf{k}) \\
&= - \sum_{\alpha, \beta} \int \frac{d^3\mathbf{p}_1}{(2\pi)^3} \frac{d^3\mathbf{p}_2}{(2\pi)^3} \frac{d^3\mathbf{k}}{(2\pi)^3} 2|\mathbf{k}| \\
&\quad \cdot \tilde{\psi}_\alpha^\dagger(\mathbf{p}_1) \tilde{\psi}_\beta(\mathbf{p}_2) \tilde{A}^\mu(\mathbf{k}) |0\rangle \langle 0| \tilde{\psi}_\beta^\dagger(\mathbf{p}_2) \tilde{\psi}_\alpha(\mathbf{p}_1) \tilde{A}_\mu(\mathbf{k})
\end{aligned} \tag{46}$$

in terms of the momentum space field operators defined in (41). Replacing $\langle 0| \rightarrow \langle \Omega|$ and using translation invariance leads to the correct normalization in the weak coupling limit

$$1 = \int \frac{d^3\mathbf{p}}{(2\pi)^3} \text{Tr} \left\{ \varphi_{\mathbf{P}}^\dagger(\mathbf{p}) \varphi_{\mathbf{P}}(\mathbf{p}) \right\} - \int \frac{d^3\mathbf{p}}{(2\pi)^3} \frac{d^3\mathbf{k}}{(2\pi)^3} 2|\mathbf{k}| \text{Tr} \left\{ \Phi_{\mathbf{P}}^{\mu\dagger}(\mathbf{p}, \mathbf{k}) \Phi_{\mathbf{P}\mu}(\mathbf{p}, \mathbf{k}) \right\} + \dots \tag{47}$$

where \dots stands for the contribution from higher Fock states and the trace is over the Dirac indices. The probability distribution for the Coulomb gauge wave function (43) (with $\Phi_{\mathbf{P}}^0 = 0$) is thus

$$\begin{aligned}
\frac{d^6\mathcal{P}}{d^3\mathbf{k}d^3\mathbf{q}}(\mathbf{q}, \mathbf{k}) &\equiv \frac{1}{(2\pi)^6} 2|\mathbf{k}| \text{Tr} \left\{ \Phi_{\mathbf{P}}^{i\dagger}(\mathbf{P}/2 + \mathbf{q}, \mathbf{k}) \Phi_{\mathbf{P}}^i(\mathbf{P}/2 + \mathbf{q}, \mathbf{k}) \right\} \\
&= \frac{\alpha}{4\pi^2} \frac{\beta^2 \mathbf{k}_\perp^2}{|\mathbf{k}|^3 (|\mathbf{k}| - \beta k_\parallel)^2} \frac{|\phi_{\mathbf{P}}(\mathbf{q}) - \phi_{\mathbf{P}}(\mathbf{q} - \mathbf{k})|^2}{(2\pi)^3}
\end{aligned} \tag{48}$$

expressed in terms of the wave function $\phi_{\mathbf{P}}$ defined in (36), (37). Inserting the distribution (48) into the normalization condition (47) and using the estimates (8) we see that the probability for this higher Fock state is $\mathcal{O}(\alpha)$. This is in accord with our above result that $\Delta t_I / \Delta t_F$ is $\mathcal{O}(\alpha)$: the fraction of time that a transverse photon is being exchanged is of $\mathcal{O}(\alpha)$. It is straightforward to repeat the analysis for even higher Fock states and check that their probability is $\mathcal{O}(\alpha^n)$ with $n \geq 2$.

3.1 The photon momentum distribution

The distribution (48) may be decomposed into three parts

$$\begin{aligned}
\frac{d^6\mathcal{P}}{d^3\mathbf{k}d^3\mathbf{q}} &= \frac{\alpha}{4\pi^2} \frac{\beta^2 \mathbf{k}_\perp^2}{|\mathbf{k}|^3 (|\mathbf{k}| - \beta k_\parallel)^2} \\
&\quad \cdot \frac{1}{(2\pi)^3} \left[|\phi_{\mathbf{P}}(\mathbf{q})|^2 + |\phi_{\mathbf{P}}(\mathbf{q} - \mathbf{k})|^2 - 2 \text{Re} \{ \phi_{\mathbf{P}}(\mathbf{q}) \phi_{\mathbf{P}}^*(\mathbf{q} - \mathbf{k}) \} \right].
\end{aligned} \tag{49}$$

In the square of the wavefunction (43) the first two terms correspond to graphs where the photon is emitted and absorbed by the same particle (see Fig. 7), and the interference comes from photon exchange. The factor which multiplies the two-particle wave functions in (49) depends only on \mathbf{k} and is basically the distribution of photons

²The contribution from $e^+e^-\gamma \rightarrow \gamma$, which is a higher order correction for a non-relativistic bound state, is not included in (46).

emitted by a single fermion. As one might expect, each of the three terms is separately infra-red divergent as $|\mathbf{k}| \rightarrow 0$, but the sum is infra-red safe as a consequence of the charge neutrality of the system. However, there is an ultra-violet divergence as $|\mathbf{k}| \rightarrow \infty$ which stems from the first two terms. For high \mathbf{k} the photon wavelength is short, and its emission is incoherent. The divergence reflects the distribution of photons emitted from a free electron.

Above we have used an asymmetric coordinate convention because of notational simplicity. To better understand the distribution, we use in this section a more natural, symmetric convention, where the momenta of the fermion, the antifermion and the photon are $\mathbf{P}/2 + \mathbf{q} - \mathbf{k}/2$, $\mathbf{P}/2 - \mathbf{q} - \mathbf{k}/2$ and \mathbf{k} , respectively. That is, we shift $\mathbf{q} \rightarrow \mathbf{q} + \mathbf{k}/2$ and thus redefine

$$\mathbf{q} \equiv \mathbf{p} - \mathbf{P}/2 - \mathbf{k}/2 \quad (50)$$

in the presence of a photon. We furthermore define the Lorentz contracted momentum variables

$$\begin{aligned} \hat{\mathbf{k}} &= (\hat{\mathbf{k}}_{\perp}, \hat{k}_{\parallel}) \equiv (\mathbf{k}_{\perp}, k_{\parallel}/\gamma) \\ \hat{\mathbf{q}} &= (\hat{\mathbf{q}}_{\perp}, \hat{q}_{\parallel}) \equiv (\mathbf{q}_{\perp}, q_{\parallel}/\gamma). \end{aligned} \quad (51)$$

In terms of these variables the distribution (48) becomes [remembering (37)]

$$\begin{aligned} \frac{d^6\mathcal{P}}{d^3\hat{\mathbf{k}}d^3\hat{\mathbf{q}}} &= \frac{\alpha}{4\pi^2} \frac{\gamma\beta^2\hat{\mathbf{k}}_{\perp}^2}{(\hat{\mathbf{k}}_{\perp}^2 + \gamma^2\hat{k}_{\parallel}^2)^{3/2} \left(\sqrt{\hat{\mathbf{k}}_{\perp}^2 + \gamma^2\hat{k}_{\parallel}^2} - \beta\gamma\hat{k}_{\parallel} \right)^2} \\ &\cdot \frac{\left| \phi_{CM}(\hat{\mathbf{q}} + \hat{\mathbf{k}}/2) - \phi_{CM}(\hat{\mathbf{q}} - \hat{\mathbf{k}}/2) \right|^2}{(2\pi)^3}. \end{aligned} \quad (52)$$

The azimuthally averaged photon distribution, integrated also over the relative momentum $\hat{\mathbf{q}}$ of the fermions, reads

$$\begin{aligned} \frac{d^2\mathcal{P}}{d\hat{k}d\cos\theta} &\equiv \hat{k}^2 \int_0^{2\pi} d\varphi \int d^3\hat{\mathbf{q}} \frac{d^6\mathcal{P}}{d\hat{\mathbf{k}}^3d\hat{\mathbf{q}}^3} \\ &= \frac{\alpha}{4\pi^2} \frac{\gamma\beta^2(1 - \cos^2\theta)}{(1 + \beta^2\gamma^2\cos^2\theta)^{3/2} \left(\sqrt{1 + \beta^2\gamma^2\cos^2\theta} - \beta\gamma\cos\theta \right)^2} \\ &\cdot \frac{1}{\hat{k}} \int_0^{2\pi} d\varphi \int \frac{d^3\hat{\mathbf{q}}}{(2\pi)^3} \left| \phi_{CM}(\hat{\mathbf{q}} + \hat{\mathbf{k}}/2) - \phi_{CM}(\hat{\mathbf{q}} - \hat{\mathbf{k}}/2) \right|^2 \end{aligned} \quad (53)$$

where θ is the angle between \mathbf{P} and $\hat{\mathbf{k}}$, φ is the remaining azimuthal angle and $\hat{k} = |\hat{\mathbf{k}}|$. Note that the frame dependence only appears in the angular distribution multiplying the integrals. An exactly Lorentz contracting distribution would be completely frame independent when expressed in terms of the variables (51). The angular distribution is the same as that of a free particle, $e \rightarrow e + \gamma$.

3.2 The photon distribution for the ground state

The photon distribution (53) is valid for any e^+e^- bound state wave function ϕ_{CM} . Let us study the ground state

$$\phi_{CM}^{(0)}(\hat{\mathbf{q}}) = \sqrt{\frac{512\pi}{\alpha^3 m^3}} \frac{1}{\left[1 + \frac{\hat{\mathbf{q}}^2}{(\alpha m/2)^2}\right]^2}. \quad (54)$$

For the wave function (54) the integral over $\hat{\mathbf{q}}$ in (53) is independent of the angles θ and φ . Thus the θ and \hat{k} dependence of the distribution completely factorizes, *i.e.*,

$$\frac{d^2\mathcal{P}}{d\hat{k} d\cos\theta} = \frac{\alpha}{2\pi} f(\cos\theta) g(\hat{k}) \quad (55)$$

where the angular dependence is

$$f(\cos\theta) \equiv \frac{\gamma\beta^2(1 - \cos^2\theta)}{(1 + \beta^2\gamma^2 \cos^2\theta)^{3/2} \left(\sqrt{1 + \beta^2\gamma^2 \cos^2\theta} - \beta\gamma \cos\theta\right)^2} \quad (56)$$

and

$$g(\hat{k}) \equiv \frac{1}{\hat{k}} \int \frac{d^3\mathbf{q}}{(2\pi)^3} \left| \phi_{CM}^{(0)}(\hat{\mathbf{q}} + \hat{\mathbf{k}}/2) - \phi_{CM}^{(0)}(\hat{\mathbf{q}} - \hat{\mathbf{k}}/2) \right|^2. \quad (57)$$

The dependence of the function f on γ in (56) gives the deviation from exact Lorentz contraction. The angular dependence is plotted for various values of γ in Fig. 8. In particular, we have

$$\beta^{-2} f(\cos\theta) \longrightarrow (1 - \cos^2\theta) \quad \text{as } \beta \rightarrow 0 \quad (58)$$

$$f(\cos\theta) \longrightarrow 4\Theta(\cos\theta) \frac{1 - \cos^2\theta}{\cos\theta} \quad \text{as } \beta \rightarrow 1 \quad (59)$$

where Θ is the step function. Thus for large boosts $\gamma \gg 1$ almost all of the photons have $k_{\parallel} > 0$.

Let us study the (frame independent) radial distribution $g(\hat{k})$ of (57). For $\hat{k} \gg \alpha m$, the interference term is negligible and we have

$$g(\hat{k}) \simeq \frac{2}{\hat{k}} \quad (60)$$

so that the distribution falls as $1/\hat{k}$ for large \hat{k} . For $\hat{k} \ll \alpha m$ we have

$$g(\hat{k}) \simeq \frac{1}{\hat{k}} \int \frac{d^3\hat{\mathbf{q}}}{(2\pi)^3} \left| \hat{\mathbf{k}} \cdot \nabla \phi_{CM}^{(0)}(\hat{\mathbf{q}}) \right|^2 = \frac{4\hat{k}}{(\alpha m)^2} \quad (61)$$

which reflects the decoupling of long wavelength photons from neutral positronium. The limit of small and large \hat{k} behaviors found here is similar for excited states of positronium.

For general values of \hat{k} the distribution $g(\hat{k})$ may be found numerically. It is also possible to study the correlation between the magnitudes of \hat{q} and \hat{k} by including a \hat{q} dependent cut in the integration of (57). This is illustrated in Fig. 9. Almost all of

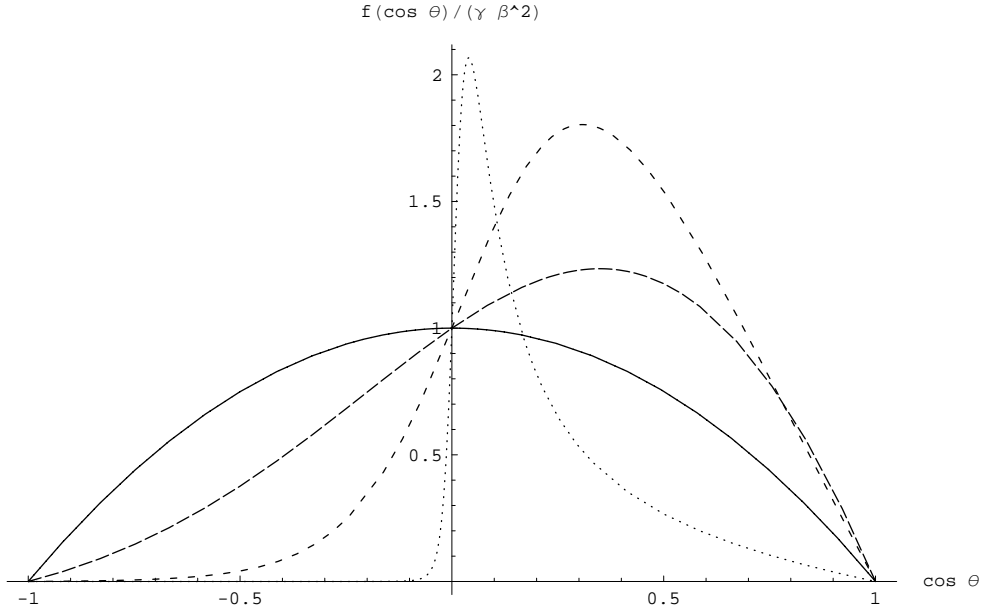


Figure 8: The angular dependence the contracted and integrated photon distribution (53) in the positronium ground state. The lines show the angular distribution $f(\cos\theta)/(\gamma\beta^2)$ [defined in (56)] for $\beta = 0.001, 0.5, 0.9$ and 0.999 . For $\beta = 0.001$ (solid line) the distribution is close to the symmetric limit (58). For $\beta = 0.999$ (dotted line) the distribution approaches the limit (59).

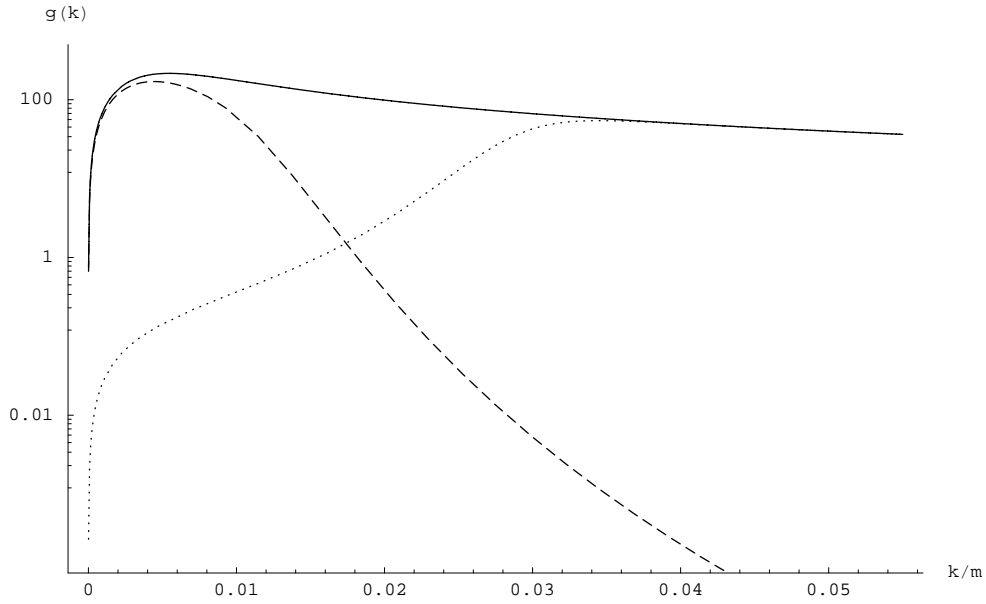


Figure 9: The radial behavior for the integrated photon distribution (53). Solid line is the function $g(\hat{k})$ defined in (57). Dashed and dotted lines are the contributions to $g(\hat{k})$ from the regions $\hat{q} < 0.7\alpha m$ and $\hat{q} > 2\alpha m$, respectively.

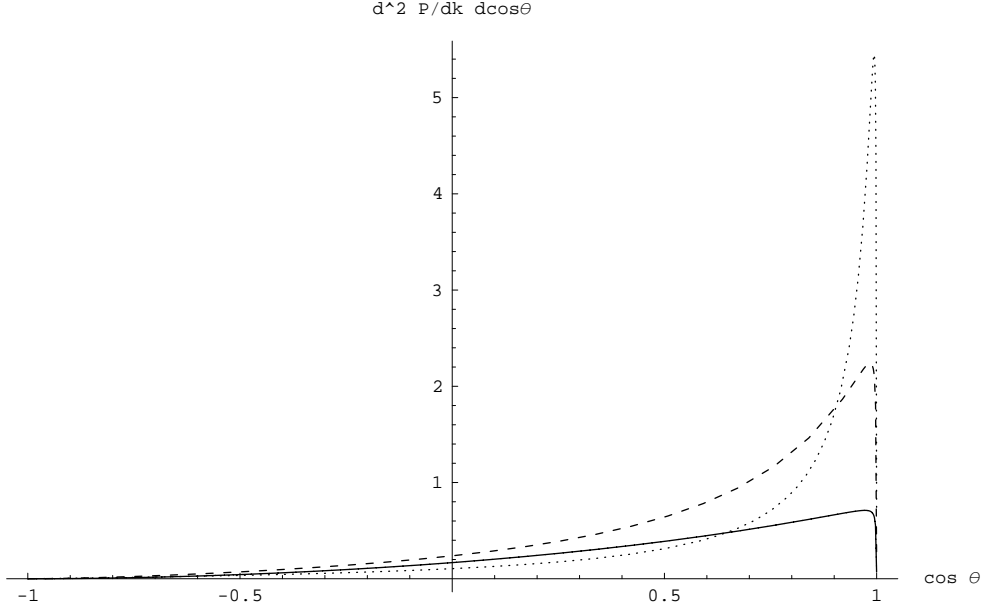


Figure 10: The angular dependence of the integrated photon distribution (62) for a system with velocity $\beta = 0.999$. Solid, dashed and dotted lines show the angular distribution for $k = 0.3\alpha m$, αm and $3\alpha m$, respectively.

the long wavelength photons $\hat{k} \ll \alpha m$ are present when the size of the fermion system (given by $1/\hat{q}$) is also large. Conversely, soft photon emission by compact fermion systems is suppressed.

It is also instructive to plot the photon distribution in terms of the usual (uncontracted) momentum variable \mathbf{k} . In terms of \mathbf{k} the integrated photon distribution (53) for the ground state becomes

$$\frac{d^2 \mathcal{P}}{dk d\cos\theta} = \frac{\alpha \beta^2 (1 - \cos^2 \theta)}{2\pi (1 - \beta \cos \theta)^2} \cdot \frac{1}{k} \int \frac{d^3 \hat{\mathbf{q}}}{(2\pi)^3} \left| \phi_{CM}^{(0)}(\hat{\mathbf{q}} + \hat{\mathbf{k}}/2) - \phi_{CM}^{(0)}(\hat{\mathbf{q}} - \hat{\mathbf{k}}/2) \right|^2 \quad (62)$$

where the integral only depends on $\hat{k} = k\sqrt{1 - \beta^2 \cos^2 \theta}$. For $\beta \rightarrow 0$ we have $\mathbf{k} = \hat{\mathbf{k}}$ and the distribution (62) coincides with the $\hat{\mathbf{k}}$ distribution described above. However, for large boosts there is a big difference between the distributions. We plot the angular distribution for different values of k in Fig. 10 for a system with $\beta = 0.999$. There is a drastic difference when compared to the contracted distribution of Fig. 8. Due to the Lorentz contraction effect, the distribution is peaked at forward angles, in particular for large k .

In our calculation (43) we assumed that $\hat{k} \sim \alpha m$. Hence the results do not necessarily hold for arbitrarily large values of \hat{k} . However, it is straightforward to check that the $1/k$ behavior is consistent with the small z behavior $\sim 1/z$ of the Weizsäcker-Williams

photon distribution function

$$f_\gamma(z) = \frac{\alpha}{2\pi} \left[\frac{1 + (1-z)^2}{z} \right] \log \frac{s}{m_e^2} \quad (63)$$

which gives the probability of finding a physical, transverse photon with a longitudinal momentum fraction z in a high energy electron (see, *e.g.*, [15]).

3.3 High $|\mathbf{P}|$ limit

Finally we check that our result for the photon distribution (48) is compatible with the light-front results. It is generally accepted that the usual equal-time picture of quantum field theory in the infinite momentum frame coincides with the one calculated at equal light-front time $x^+ = t + z = 0$. Thus to compare with the light-front results, we need to take the limit $|\mathbf{P}| \rightarrow \infty$. It is easy to check that in this limit our solutions for the e^+e^- wave function (37) reduce to the light-front wave functions at leading order in α (see [12, 16]),

$$\phi_{\mathbf{P}}(\mathbf{q}) = \sqrt{\frac{(2\pi)^3}{|\mathbf{P}|}} \phi_{LF}(y, \mathbf{q}_\perp) \left[1 + \mathcal{O}\left(\frac{m}{|\mathbf{P}|}\right) \right], \quad (64)$$

where y is the momentum fraction $y \equiv p_\parallel/|\mathbf{P}| \simeq 1/2 + q_\parallel/2\gamma m$. As the two-particle Fock state is leading in α also on the light front the normalization can be taken to be $1 = \int d\mathbf{p}_\perp \int_0^1 dy |\phi_{LF}(y, \mathbf{p}_\perp)|^2$.

The light-front photon distribution is calculated in [12]. As in our calculation the probability of the Fock state with one additional photon is $\mathcal{O}(\alpha)$. To compare with our result we need the relations

$$\begin{aligned} |\mathbf{k}| &= |\mathbf{P}||x| \left[1 + \mathcal{O}\left(\frac{m}{|\mathbf{P}|}\right) \right] \\ \frac{1}{|\mathbf{k}| - \beta k_\parallel} &= \Theta(x) \frac{2|\mathbf{P}|x}{(2mx)^2 + \mathbf{k}_\perp^2} \left[1 + \mathcal{O}\left(\frac{m}{|\mathbf{P}|}\right) \right]. \end{aligned} \quad (65)$$

where x is the momentum fraction $x \equiv k_\parallel/|\mathbf{P}| \simeq k_\parallel/2\gamma m$. Note that (8) gives

$$x \sim \alpha \sim \left(y - \frac{1}{2} \right). \quad (66)$$

Inserting (64) and (65) into (48) we find

$$\begin{aligned} \mathbf{P}^2 \frac{d^6\mathcal{P}}{d^3\mathbf{k}d^3\mathbf{q}}(\mathbf{q}, \mathbf{k}) &\longrightarrow \frac{d^6\mathcal{P}}{dyd^2\mathbf{k}_\perp dx d^2\mathbf{q}_\perp}(x, \mathbf{k}_\perp, y, \mathbf{q}_\perp) \\ &= \frac{\alpha}{\pi^2} \Theta(x) \frac{\mathbf{k}_\perp^2/x}{[(2mx)^2 + \mathbf{k}_\perp^2]^2} |\phi_{LF}(y, \mathbf{q}_\perp) - \phi_{LF}(y-x, \mathbf{q}_\perp - \mathbf{k}_\perp)|^2 \end{aligned} \quad (67)$$

which agrees with the light-front result [12]³.

³The result (67) is missing the constraints $x < y < 1$ which appear at the light front. They are unimportant in the weak coupling limit as $x \sim \alpha$ and the light-front wave functions are peaked at $y \simeq 1/2$.

4 Summary and discussion

We studied the frame dependence of non-relativistic QED bound states such as positronium or the hydrogen atom. Starting from the exact field theoretical Bethe-Salpeter equation we evaluated the wave function to leading order in α in all Lorentz frames. Using a time-ordered formalism we confirmed the expected result: the e^+e^- equal-time wave functions exactly Lorentz contract in boosts while the mass spectrum is invariant.

We also solved the leading component of the wave function of the $e^+e^-\gamma$ Fock state. We saw that this Fock state was a next-to-leading correction with a probability $\mathcal{O}(\alpha)$. The resulting photon distribution did not contract exactly in boosts, similarly to the radiation from a single electron, $e \rightarrow e + \gamma$. The infinitely boosted limit of the distribution was seen to coincide with light-front results.

The “old-fashioned” time-ordered approach is natural when considering wave functions evaluated at equal time. The advantages of the time-ordered formalism for bound states are well known from studies of positronium in the center-of-mass frame – see, *e.g.*, [17] and references therein. In our case the time-ordering was helpful in the analysis of the Fock state structure of the bound state and in determining the correct order of α for various interaction kernels.

The covariant (four-dimensional) form of the Bethe-Salpeter equation determines also the dependence on the relative time t of the bound state constituents. The time dependent wave function $\Psi(t, \mathbf{x})$ may be derived at weak coupling as in the 1+1 dimensional case studied in section II.C of [10]. The result is⁴

$$\Psi_{\mathbf{P}}(t, \mathbf{x}) = \exp\left(-\frac{i\alpha|t|}{2\gamma\sqrt{\mathbf{x}_{\perp}^2 + \gamma^2\tilde{x}_{\parallel}^2}}\right) \tilde{\varphi}_{\mathbf{P}}(\tilde{x}_{\parallel}, \mathbf{x}_{\perp}) \quad (68)$$

where $\tilde{x}_{\parallel} \equiv x_{\parallel} - \beta t$ is the longitudinal distance between the constituents adjusted for the displacement $\beta t = |\mathbf{P}|t/E$ of the center of mass, and $\tilde{\varphi}_{\mathbf{P}}$ is the equal-time wave function $\varphi_{\mathbf{P}}$ of (36) Fourier transformed to coordinate space. Combining (68) with our result (36) one may check that the covariant Lorentz transformation formula [1] of the e^+e^- wave function is satisfied,

$$\Psi_{\mathbf{P}'}(t', \mathbf{x}') = S(\Lambda)\Psi_{\mathbf{P}=0}(t, \mathbf{x})S^{-1}(\Lambda) \quad (69)$$

where $S(\Lambda)$ is the standard spin transformation matrix of the Dirac equation.

It would be interesting to extend the analysis presented here to the next-to-leading order in α and check if the correction to the wave function contracts classically. Likewise one could consider the frame dependence of non-relativistic bound states in other theories, *e.g.*, for states bound by scalar exchange.

In previous work scant attention has been paid to the description of moving bound states in field theory, even though much is known about the center-of-mass frame solutions, in particular for non-relativistic systems. However, the problem is non-trivial and certainly worth studying. The usual center-of-mass equal-time wave functions are related by an infinite boost to the light-front wave functions which appear in the

⁴The time dependence in the case of non-relativistic center-of-mass motion was given in [9, 18].

parton model. Hence a better understanding of the behavior of (relativistic) bound states under boosts could help to relate the non-relativistic quark model and the parton model of hadrons. Evaluating the boosted wave functions of the simpler, non-relativistic systems which we studied here is a first step towards understanding the boost properties of relativistic systems such as hadrons.

Acknowledgments

I would like to thank Paul Hoyer for suggesting this topic and for several useful discussions. I am also grateful for Paul Hoyer and Stanley Brodsky for comments on the paper.

References

- [1] S. J. Brodsky and J. R. Primack, *Ann. Phys.* **52**, 315 (1969); S. J. Brodsky, *Brandeis Lectures 1969, Vol 1*, (Gordon and Breach, New York, 1971).
- [2] W. Glöckle and Y. Nogami, *Phys. Rev.* **D35**, 3840 (1987).
- [3] P. Hoyer, *Phys. Lett.* **B172**, 101 (1986).
- [4] V. Schon and M. Thies, hep-th/0008175.
- [5] W. Glöckle, Y. Nogami, and I. Fukui, *Phys. Rev.* **D35**, 584 (1987).
- [6] F. Guinea, R. E. Peierls and R. Schrieffer, *Physica Scripta* **33** 282 (1986).
- [7] A. J. Hanson, R. D. Peccei and M. K. Prasad, *Nucl. Phys.* **B121**, 477 (1977).
- [8] X. Artru, *Phys. Rev.* **D29**, 1279 (1984).
- [9] E. E. Salpeter and H. A. Bethe, *Phys. Rev.* **84**, 1232 (1951).
- [10] M. Järvinen, *Phys. Rev.* **D70**, 065014 (2004).
- [11] E. E. Salpeter, *Phys. Rev.* **87**, 328 (1952).
- [12] M. Burkardt, *Nucl. Phys.* **B373**, 371 (1992).
- [13] S. J. Brodsky and J. F. Gunion, *Phys. Rev.* **D19**, 1005 (1979).
- [14] N. Nakanishi, *Prog. Theor. Phys. (Kyoto) Suppl.* **43**, 1 (1969).
- [15] M. Peskin and D. Schroeder, *An Introduction to Quantum Field Theory*, (Addison-Wesley, 1997), p. 578.
- [16] G. P. Lepage and S. J. Brodsky, *Phys. Rev.* **D22**, 2157 (1980), appendix A.
- [17] P. Labelle, *Phys. Rev.* **D58**, 093013 (1998).
- [18] C. Hayashi and Y. Munakata, *Prog. Theor. Phys.* **7**, 481 (1952).